Large molecular gas reservoirs in ancestors of Milky Way-mass galaxies nine billion years ago

Papovich, C.; Labbé, I.F.L.; Glazebrook, K.; Quadri, R.; Bekiaris, G.; Dickinson, M.; ... ; Tran, K.

LETTER

Large Molecular Gas Reservoirs in Ancestors of Milky Way-Mass Galaxies 9 Billion Years Ago

C. Papovich[1,2], I. Labbé[3], K. Glazebrook[4], R. Quadri[1,2], G. Bekiaris[4], M. Dickinson[5], S. L. Finkelstein[6], D. Fisher[4], H. Inami[5,7], R. C. Livermore[6], L. Spitler[8,9], C. Straatman[3], K.-V. Tran[1,2]

The gas accretion and star-formation histories of galaxies like the Milky Way remain an outstanding problem in astrophysics.[1,2] Observations show that 8 billion years ago, the progenitors to Milky Way-mass galaxies were forming stars 30 times faster than today and predicted to be rich in molecular gas,[3] in contrast with low present-day gas fractions (<10%).[4–6] Here we show detections of molecular gas from the CO(J=3–2) emission (rest-frame 345.8 GHz) in galaxies at redshifts z=1.2–1.3, selected to have the stellar mass and star-formation rate of the progenitors of today's Milky Way-mass galaxies. The CO emission reveals large molecular gas masses, comparable to or exceeding the galaxy stellar masses, and implying most of the baryons are in cold gas, not stars. The galaxies' total luminosities from star formation and CO luminosities yield long gas-consumption timescales. Compared to local spiral galaxies, the star-formation efficiency, estimated from the ratio of total IR luminosity to CO emission, has remained nearly constant since redshift z=1.2, despite the order of magnitude decrease in gas fraction, consistent with results for other galaxies at this epoch.[7–10] Therefore the physical processes that determine the rate at which gas cools to form stars in distant galaxies appear to be similar to that in local galaxies.

Studies of the distribution of stellar ages and elemental abundances in the Milky Way and M31 conclude most of their stars formed in the distant past, more than 7 billion years ago.[11,12] This agrees with recent work that shows star-formation in present-day galaxies with the mass of the Milky Way peaked more than 8 billion years ago, at $z>1$,[3] with star-formation rates (SFRs) exceeding 30 $M_\odot$ yr^{-1}, compared to a present day SFR of 1.7±0.2 $M_\odot$ yr^{-1} for the Milky Way.[13]

Theoretical models explain periods of high star formation as a result of rapid baryonic gas accretion from the intergalactic medium (IGM), which leads to high cold gas concentrations in galaxies at earlier times.[14] These models predict that the gas settles into rotationally supported, highly turbulent disks, which fragment to form stars.[15] Observations of star-forming galaxies at $z>1$ (stellar masses, $M_*>2\times10^{10}$ $M_\odot$) show evidence for gas-rich, rotating disks,[16–19] supporting these theories. However, the situation is far from settled for lower mass ($M_* \sim 10^{10}$ $M_\odot$), more common galaxies such as the progenitors to the Milky Way. Some models predict that these galaxies should experience early, rapid star formation, leaving low gas fractions (<10%) at redshifts $z\sim1$.[20] Others predict that the gas flows from the IGM can perturb and disrupt the formation of disk instabilities, thereby suppressing star formation in galaxies and extending star-formation histories.[21,22] The first step to understand star formation in galaxies like the Milky Way is to measure the amount of the cold gas in their progenitors at $z>1$. As the gas is the fuel for star formation, the ratio of the SFR to gas mass can test the physical processes in the models.[23]

With the greatly improved sensitivity offered by the Atacama Large Millimeter Array (ALMA), we are able now to explore the evolution of cold molecular gas in low mass galaxies at redshifts $z > 1$. With ALMA, we observed the J=3 to 2 transition of CO in four galaxies with the stellar mass and SFR expected of the main progenitors to present-day Milky Way-mass galaxies at redshifts $z = 1.2 - 1.3$ selected from deep imaging by the FourStar Galaxy Evolution (ZFOURGE) survey[24] (see discussion in the Methods). Figure 1 shows the integrated emission from the CO $J = 3$ to 2 transition in these galaxies, where the detections range in significance from 4.8–13.7σ (r.m.s.). The CO(3–2) emission coincides with the spatial positions of the galaxies in Hubble Space Telescope (HST) imaging (Figure 1); the small offsets are consistent with astrometric calibrations and ALMA beam smearing. Table 1 gives the measured properties of these galaxies. The ALMA detections of CO emission probe the molecular mass in galaxies with the stellar mass and SFRs that the main progenitor of the Milky Way was expected to have ∼8.5 billion years ago. This provides an important extension of previous work, as the galaxies in our sample have lower stellar masses and SFRs than have been generally possible to study at these redshifts.[10]

CO is the most luminous tracer of molecular hydrogen (H_2), the fuel for star formation. The CO specific intensity from the J to J–1 transition, $I_{\rm CO(J-[J-1])}$, is a function of both the gas density and temperature. In high redshift galaxies, studies show that the average excitation of CO(3–2) is similar to that of star-forming regions in the Milky Way,[27] and we assume an integrated Rayleigh–Jeans brightness temperature line ratio, $r_{31} = I_{\rm CO(3-2)}/I_{\rm CO(1-0)} \times (1/3)^2 = 0.66$.[26] The total CO luminosity in the J=1 to 0 transition is then $L'_{\rm CO} = 3.25\times10^7\ r_{31}^{-1}\ I_{\rm CO(3-2)}\ \nu_{\rm obs}^{-2}\ D_L^2\ (1+z)^{-3}$ where $\nu_{\rm obs}$ is the frequency (in GHz) of the CO emission in the observed frame and D_L is the luminosity distance in Mpc. Table 1 displays the $L'({\rm CO})$ values. Using lower values of $r_{31} \sim 0.4-0.5$, as indicated by some other studies of star-forming galaxies at $z\sim1$–2, [27,28] would increase the $L'({\rm CO})$ values slightly but not change our conclusions.

The combination of the CO luminosity and the luminosity from newly formed stars provides a crucial constraint on the star-formation efficiency (SFE). We use the thermal IR luminosity ($L_{\rm IR}$, measured over 8–1000 μm in the rest frame), which originates from dust in dense molecular clouds heated by young stars, and is directly proportional to the total SFR. We measured $L_{\rm IR}$ for galaxies in our study using model fits to fluxes measured from *Spitzer Space Telescope* and *Her-*

[1]George P. and Cynthia Woods Mitchell Institute for Fundamental Physics and Astronomy, Texas A&M University, College Station, Texas 78743, USA [2]Department of Physics and Astronomy, Texas A&M University, 4242 TAMU, College Station, TX 78743, USA [3]Leiden Observatory, Leiden University, P.O. Box 9513, 2300 RA Leiden, The Netherlands [4]Centre for Astrophysics & Supercomputing, Swinburne University, Hawthorn, VIC 3122, Australia [5]National Optical Astronomy Observatory, Tucson, AZ 85719, USA [6]Department of Astronomy, The University of Texas at Austin, 2515 Speedway, Stop C1400, Austin, TX 78712, USA [7]Centre de Recherche Astrophysique de Lyon, Université de Lyon, Université Lyon 1, CNRS, Observatoire de Lyon, 9 avenue Charles André, F-69561 Saint-Genis Laval Cedex, France [8]Department of Physics & Astronomy, Macquarie University, Sydney, NSW 2109, Australia [9]Australian Astronomical Observatory, PO Box 915, North Ryde, NSW 1670, Australia

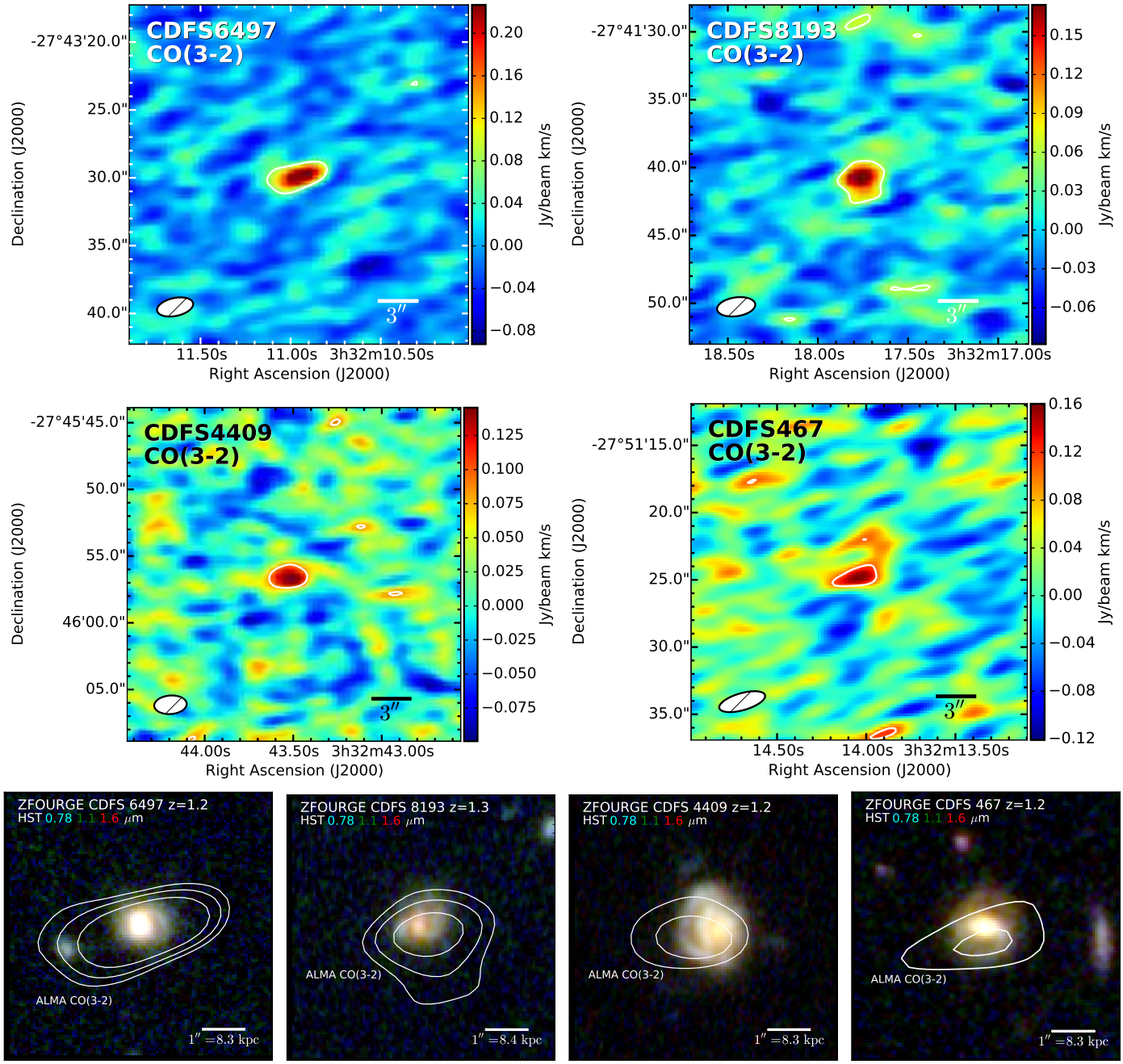

Figure 1 | Images of Milky Way Progenitors at redshifts z = 1.2 to 1.3. The top panels show the ALMA images of the redshifted CO J=3–2 emission for each galaxy. The inset bar shows a scale length of 3 arcseconds, and the hashed ellipse shows the size of the synthesized ALMA beam of each observation. The contours denote the emission at 2 times the noise. The bottom panels show combined Hubble Space Telescope images at 0.78, 1.1, and 1.6 μm (approximately the rest-frame U–, V–, and R–band emission). The contours denote ALMA CO(3-2) emission with levels at 2, $2\sqrt{2}$, and 4 times the noise. The inset bar shows a scale length of 1 arcsecond, which corresponds to a physical scale of 8.3–8.4 kpc at these redshifts.

Table 1 | Properties of Progenitors of Milky-Way-Mass Galaxies at $z = 1.2 - 1.3$

ZFOURGE ID	$z_{\rm opt}$ [a]	$z_{\rm CO}$ [b]	R.A. [c] (deg.)	Decl. [d] (deg.)	$I_{\rm CO(3-2)}$ [e] (Jy km s^{-1})	$L'_{\rm CO}$ [f] (10^9 K km s^{-1} pc^2)	$M_{\rm gas}$ [†] (10^{10} $M_\odot$)	$L_{\rm IR}$ [g] (10^{11} $L_\odot$)	M_* [‡] (10^{10} $M_\odot$)
CDFS 467	1.220	1.221	53.05850	−27.85678	0.11(0.05)	1.4(0.6)	0.55(0.19)	1.5(0.1)	$2.2^{+0.4}_{-0.8}$
CDFS 4409	1.220	1.220	53.18124	−27.76566	0.25(0.06)	3.3(0.8)	1.4 (0.4)	3.1(0.1)	$1.7^{+0.3}_{-0.3}$
CDFS 6497	1.215	1.215	53.04564	−27.72493	0.33(0.04)	4.3(0.6)	2.3 (0.3)	2.3(0.3)	$2.0^{+0.3}_{-0.5}$
CDFS 8193	1.326	1.326	53.07405	−27.69459	0.31(0.05)	4.9(0.8)	2.0 (0.4)	2.2 (0.3)	$1.9^{+0.1}_{-0.2}$

Numbers in parentheses are 1σ uncertainties. [a]Redshift from optical spectroscopy.[25] [b]Redshift measured from ALMA CO(3–2) data (see Methods). [c]Right Ascension and [d]Declination (J2000). [e]CO(3–2) flux density. [f]CO luminosity, converted to the CO J=1 to 0 transition assuming r_{31}=0.66.[26] [†]Total molecular gas mass in H_2 (see Methods). [g]Total IR luminosity from 8–1000 μm (see Methods). [‡]Stellar mass measurements (see Methods).

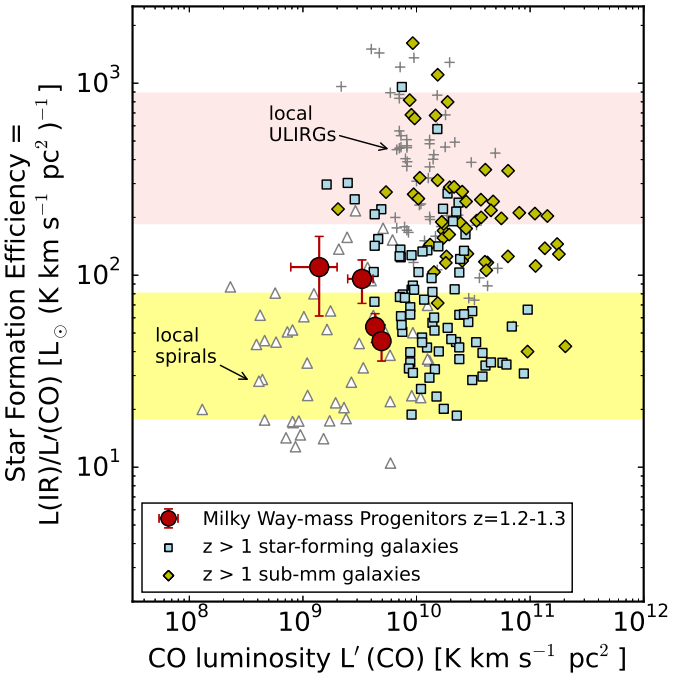

Figure 2 | Star Formation Efficiency as a function of CO luminosity, $\mathbf{L'(CO)}$. The star-formation efficiency is defined as the ratio of the total IR luminosity ($L_{\rm IR}$) to $L'({\rm CO})$, where $L'({\rm CO})$ is converted to the emission of the J=1–0 transition. The $z = 1.2 - 1.3$ galaxies in our sample are shown as large red circles. Error bars denote 1σ uncertainties. Other small symbols denote control samples of star-forming galaxies, including local spiral galaxies (open triangles), local ultraluminous IR galaxies (ULIRGS; crosses),[29–31] high redshift ($z > 1$) star-forming galaxies (cyan-filled squares), and high redshift submillimetre galaxies (yellow-filled diamonds).[10,32] The shaded regions show the interquartile ranges of the star-formation efficiency for local normal spirals and ULIRGs.

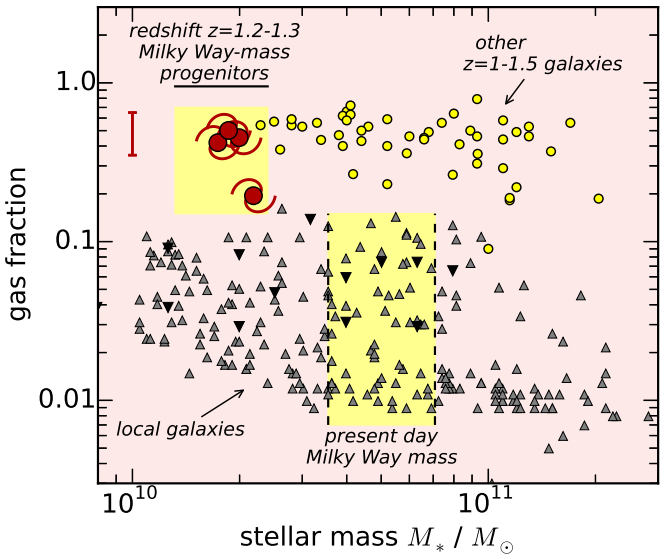

Figure 3 | The relation between the molecular gas fraction and total stellar mass in galaxies at $\mathbf{z = 1 - 1.5}$ compared to local galaxies. Here the gas fraction is defined as the ratio $M_{\rm gas}/(M_{\rm gas} + M_*)$. The progenitors of Milky Way-mass galaxies at $z = 1.2 - 1.3$ are denoted by large, red spirals. The red bar shows the typical statistical uncertainty, ≈30%.. Smaller, yellow circles show other galaxies at $z = 1 - 1.5$.[7,9,10] The smaller triangles show measurements for local ($z \sim 0$) galaxies with data from the literature, including COLD GASS[6] (gray, upward triangles) and the HERA CO line excitation survey[5] (black, downward triangles). The region separated by vertical dashed lines shows the stellar mass range of Milky Way–like galaxies at present.

schel Space Observatory imaging covering 24–250 μm (see Methods). Table 1 displays these values. They span $L_{\rm IR}$=$(1.5 - 2.7)\times10^{11}$ $L_\odot$ (corresponding to SFRs of 15–30 $M_\odot$ yr^{-1}). Uncertainties are ≃0.2 dex (60%) and are dominated by systematics from differences in the IR model (see Methods).

Figure 2 shows the SFE, defined as $L_{\rm IR}/L'({\rm CO})$, as a function of $L'({\rm CO})$ for the z=1.2–1.3 galaxies in our sample compared to control samples. With ALMA we now probe efficiently the CO luminosities of $z > 1$ star-forming galaxies a factor two lower than was possible previously. The galaxies in our sample have SFEs typical of the upper range of both local spiral galaxies and more massive, high-redshift star-forming galaxies. In such galaxies, star-formation occurs in rotationally supported disks. In at least two of our galaxies, the CO(3–2) spectra show strongly double–peaked line profiles (see Methods). This and the apparent presence of spatial velocity shear (see Methods) observed in our analysis of the CO data suggests that the same may be true for all the z=1.2-1.3 galaxies in our sample. Therefore, even though both the SFRs and gas fractions are substantially higher in these distant galaxies, their star formation likely occurs in rotating disks, where the physical processes governing the evolution of the gas appears to be similar to that of spiral galaxies in the local Universe. In contrast, the SFEs of more luminous, rarer objects (ULIRGs, QSOs, and submillimetre galaxies [SMGs]) are significantly enhanced in the local and distant Universe. A prevailing theory is that ULIRGs, QSOs, and SMGs are a result of increased gas densities from major gas-rich mergers.[33] These conditions seem inconsistent with the galaxies in our sample, suggesting that major mergers are not common amongst the main progenitors of Milky Way-mass galaxies at z≃1.2–1.3.

The inverse of the SFE is proportional to the gas consumption timescale, which corresponds to a range of 200 to 700 Myr for the galaxies in our sample. In contrast, the consumption timescales for ULIRGs, QSOs, and SMGs are less than 10 Myr.[32] Star-formation in the average, main progenitor of Milky Way galaxies at z=1.2–1.3 appears to be long lasting, and comparable to findings for other star-forming disk galaxies at high redshifts.[7–10,18]

The CO luminosities imply very high molecular gas fractions for the galaxies in our sample at z=1.2–1.3, where we adopt the ratio of CO luminosity to mass in H_2 gas ($M_{\rm gas}$) for Galactic star-forming regions because the SFEs are similar (see Methods). Table 1 lists these values. Figure 3 shows the molecular gas fractions ($f_{\rm gas} = M_{\rm gas} / (M_{\rm gas} + M_*)$) derived from CO observations as a function of the stellar mass, M_*. While present day Milky Way–sized galaxies have low gas fractions, $f_{\rm gas} < 10\%$, the results from our sample imply that the main progenitors to these galaxies at $z = 1.2 - 1.3$ have much higher values: in three of the galaxies in our sample, the molecular gas mass is greater than or equal to the stellar mass ($f_{\rm gas} \gtrsim 50\%$). This is consistent with indirect gas fractions of galaxies at these redshifts inferred from the thermal dust emission.[18,34] This argues against models with early, rapid gas consumption [20] and favours longer lasting, feedback–regulated star-formation.[21–23]

The high molecular gas fractions and SFRs of the z=1.2–1.3 galaxies in our sample imply they will double their stellar mass within the gas-consumption timescale. Therefore, at z∼1.2 these galaxies have most, but not all, of the fuel needed to produce the $M_* \simeq 5\times10^{10}$ $M_\odot$ in stars in Milky Way-mass galaxies at present (see Figure 3). The average baryon accretion rate from the IGM must exceed 6 $M_\odot$ yr^{-1} at earlier times (z>1.2) to account for the galaxies' total stellar and molecular masses. In constrast, the galaxies need only acquire ∼30–50% more baryonic mass from z∼1 to the present (even accounting for losses from stellar evolution), which corresponds to an average gas accretion rate of only ∼1–2 $M_\odot$ yr^{-1}. This reflects a dwindling supply

of fresh baryonic gas. Therefore, Milky Way-mass galaxies appear to accrete most of their gas at $z>1.2$, during the first few billion years of history.

1. Guedes, J., Callegari, S., Madau, P. & Mayer, L. Forming Realistic Late-type Spirals in a ΛCDM Universe: The Eris Simulation. *Astrophys. J.* **742**, 76 (2011).
2. Martig, M., Bournaud, F., Croton, D. J., Dekel, A. & Teyssier, R. A Diversity of Progenitors and Histories for Isolated Spiral Galaxies. *Astrophys. J.* **756**, 26 (2012).
3. Papovich, C. *et al.* ZFOURGE/CANDELS: On the Evolution of M* Galaxy Progenitors from z = 3 to 0.5. *Astrophys. J.* **803**, 26 (2015).
4. Sage, L. J. Molecular Gas in Nearby Galaxies I. CO Observations of a Distance-Limited Sample. *Astron. Astrophys.* **272**, 123 (1993).
5. Leroy, A. K. *et al.* Heracles: The HERA CO Line Extragalactic Survey. *Astron. J.* **137**, 4670–4696 (2009).
6. Saintonge, A. *et al.* COLD GASS, an IRAM legacy survey of molecular gas in massive galaxies - I. Relations between H_2, H I, stellar content and structural properties. *Mon. Not. R. Astron. Soc.* **415**, 32–60 (2011).
7. Daddi, E. *et al.* Very High Gas Fractions and Extended Gas Reservoirs in z = 1.5 Disk Galaxies. *Astrophys. J.* **713**, 686–707 (2010).
8. Magdis, G. E. *et al.* The Molecular Gas Content of z = 3 Lyman Break Galaxies: Evidence of a Non-evolving Gas Fraction in Main-sequence Galaxies at z > 2. *Astrophys. J. Let.* **758**, L9 (2012).
9. Magnelli, B. *et al.* Dust temperature and CO — H_2 conversion factor variations in the SFR-M plane. *Astron. Astrophys.* **548**, A22 (2012).
10. Tacconi, L. J. *et al.* Phibss: Molecular Gas Content and Scaling Relations in z ˜ 1-3 Massive, Main-sequence Star-forming Galaxies. *Astrophys. J.* **768**, 74 (2013).
11. Snaith, O. N. *et al.* The Dominant Epoch of Star Formation in the Milky Way Formed the Thick Disk. *Astrophys. J. Let.* **781**, L31 (2014).
12. Bernard, E. J. *et al.* The spatially-resolved star formation history of the M31 outer disc. *Mon. Not. R. Astron. Soc.* **453**, L113–L117 (2015).
13. Licquia, T. C. & Newman, J. A. Improved Estimates of the Milky Way's Stellar Mass and Star Formation Rate from Hierarchical Bayesian Meta-Analysis. *Astrophys. J.* **806**, 96 (2015).
14. De Lucia, G. *et al.* Elemental abundances in Milky Way-like galaxies from a hierarchical galaxy formation model. *Mon. Not. R. Astron. Soc.* **445**, 970–987 (2014).
15. Dekel, A. *et al.* Cold streams in early massive hot haloes as the main mode of galaxy formation. *Nature* **457**, 451–454 (2009).
16. Genzel, R. *et al.* The rapid formation of a large rotating disk galaxy three billion years after the Big Bang. *Nature* **442**, 786–789 (2006).
17. Tacconi, L. J. *et al.* High molecular gas fractions in normal massive star-forming galaxies in the young Universe. *Nature* **463**, 781–784 (2010).
18. Genzel, R. *et al.* Combined CO and Dust Scaling Relations of Depletion Time and Molecular Gas Fractions with Cosmic Time, Specific Star-formation Rate, and Stellar Mass. *Astrophys. J.* **800**, 20 (2015).
19. Wisnioski, E. *et al.* The KMOS^{3D} Survey: Design, First Results, and the Evolution of Galaxy Kinematics from 0.7 <= z <= 2.7. *Astrophys. J.* **799**, 209 (2015).
20. Ceverino, D., Dekel, A. & Bournaud, F. High-redshift clumpy discs and bulges in cosmological simulations. *Mon. Not. R. Astron. Soc.* **404**, 2151–2169 (2010).
21. Genel, S., Dekel, A. & Cacciato, M. On the effect of cosmological inflow on turbulence and instability in galactic discs. *Mon. Not. R. Astron. Soc.* **425**, 788–800 (2012).
22. Gabor, J. M. & Bournaud, F. Delayed star formation in high-redshift stream-fed galaxies. *Mon. Not. R. Astron. Soc.* **437**, L56–L60 (2014).
23. Agertz, O. & Kravtsov, A. V. On the Interplay between Star Formation and Feedback in Galaxy Formation Simulations. *Astrophys. J.* **804**, 18 (2015).
24. Straatman, C. M. S. *et al.* The Fourstar Galaxy Evolution Survey: ultraviolet to far-Infrared catalogs, medium-bandwidth photometric redshifts, and stellar population properties; analysis of photometric redshift accuracy and confirmation of quiescent galaxies to z∼3.5. *Astrophys. J., submitted* (2016).
25. Vanzella, E. *et al.* The great observatories origins deep survey. VLT/FORS2 spectroscopy in the GOODS-South field: Part III. *Astron. Astrophys.* **478**, 83–92 (2008).
26. Bolatto, A. D. *et al.* High-resolution Imaging of PHIBSS z ∼ 2 Main-sequence Galaxies in CO J = 1–0. *Astrophys. J.* **809**, 175 (2015).
27. Daddi, E. *et al.* CO excitation of normal star-forming galaxies out to z = 1.5 as regulated by the properties of their interstellar medium. *Astron. Astrophys.* **577**, A46 (2015).
28. Aravena, M. *et al.* CO(1-0) line imaging of massive star-forming disc galaxies at z=1.5-2.2. *Mon. Not. R. Astron. Soc.* **442**, 558–564 (2014).
29. Gao, Y. & Solomon, P. M. The Star Formation Rate and Dense Molecular Gas in Galaxies. *Astrophys. J.* **606**, 271–290 (2004).
30. Combes, F. *et al.* Galaxy evolution and star formation efficiency at 0.2 < z < 0.6. *Astron. Astrophys.* **528**, A124 (2011).
31. Combes, F. *et al.* Gas fraction and star formation efficiency at z < 1.0. *Astron. Astrophys.* **550**, A41 (2013).
32. Carilli, C. L. & Walter, F. Cool Gas in High-Redshift Galaxies. *Annu. Rev. Astron. Astrophys.* **51**, 105–161 (2013).
33. Casey, C. M., Narayanan, D. & Cooray, A. Dusty star-forming galaxies at high redshift. *Phys. Rep.* **541**, 45–161 (2014).
34. Scoville, N. *et al.* ISM Masses and the Star formation Law at z=1 to 6: ALMA Observations of Dust Continuum in 145 Galaxies in the COSMOS Survey Field. *Astrophys. J.* **820**, 83 (2016).

Acknowledgements The authors thank their colleagues on the CANDELS and ZFOURGE surveys, for providing high quality data products. The authors thank the ALMA staff for facilitating the observations, and aiding in the calibration and reduction process. The authors also wish to acknowledge the anonymous reviewers for their careful reading, valued comments, and constructive criticism. The authors acknowledge generous support from the Mitchell Institute for Fundamental Physics and Astronomy at Texas A&M University. This paper makes use of the following ALMA data: ADS/JAO.ALMA#2011.0.01234.S . ALMA is a partnership of ESO (representing its member states), NSF (USA) and NINS (Japan), together with NRC (Canada), NSC and ASIAA (Taiwan), and KASI (Republic of Korea), in cooperation with the Republic of Chile. The Joint ALMA Observatory is operated by ESO, AUI/NRAO and NAOJ. The National Radio Astronomy Observatory is a facility of the National Science Foundation operated under cooperative agreement by Associated Universities, Inc.

Author Contributions C. Papovich led the ALMA observing programme, handled the data reduction, and led the writing of the text of the manuscript. Coauthors I. Labbé, K. Glazebrook, R. Quadri, L. Spitzer, C. Straatman, and K.-V. Tran contributed extensively to the ZFOURGE dataset, used in much of the analysis. Coauthors S. Finkelstein, D. Fisher, and R. Livermore contributed to the design of the ALMA observing programme, and assisted in the ALMA data reduction and interpretation. Coauthors G. Bekiaris and K. Glazebrook assisted in the interpretation of the ALMA data. Coauthors M. Dickinson and H. Inami carried out the data analysis of the *Spitzer* and *Herschel* imaging. All co-authors contributed to the writing of the manuscript, and to the ALMA observing programme.

Author Information Reprints and permissions information is available at www.nature.com/reprints. The authors declare no competing financial interests. Readers are welcome to comment on the online version of the paper. Correspondence and requests for materials should be addressed to C.P. (papovich@tamu.edu).

Data Availability Statement The data that support the plots within this paper and other findings of this study are available from the corresponding author upon reasonable request. Data from the ZFOURGE survey can be obtained from http://zfourge.tamu.edu/

METHODS

1 ZFOURGE Dataset

We selected the galaxies in our sample from the Fourstar Galaxy Evolution (ZFOURGE) survey[24]. The main ZFOURGE survey obtained very deep near-infrared imaging in five medium–band filters (J_1, J_2, J_3, H_s, H_l) from the FourStar instrument[35] on the Magellan Baade 6.5 m telescope in the three southern fields covered by CANDELS *HST* imaging.[36,37] The ZFOURGE catalogues combine the FourStar images with ancillary ground-based imaging (spanning 0.3 – 2.5 μm), the CANDELS *HST*/ACS and WFC3 imaging, and Spitzer/IRAC imaging (spanning 3.6 – 8.0 μm). For this study, we selected targets from the earlier, version 2.1 ZFOURGE catalogues. These include photometric redshifts and stellar masses estimated from the multiwavelength catalogues as described elsewhere.[3,38] Of interest here, the catalogues are complete for objects with limiting stellar masses $\log M/M_\odot \geq 9.0 - 9.2$ in the redshift range $1.0 < z < 1.5$, well below the stellar masses of the typical progenitor of a Milky-Way-mass galaxy.[3]

2 Selection of Milky-Way-Mass Galaxy Progenitors

We selected galaxies as targets for ALMA observations of the CO(J=3 to 2) transition that have the typical stellar mass and SFR of progenitors to Milky Way-mass galaxies at $z = 1.2 - 1.3$. We identified progenitors of galaxies with the present-day stellar mass of a Milky Way-mass galaxy ($M_* = 5\times10^{10}$ $M_\odot$ at $z = 0$)[13,39] using abundance-matching techniques.[40] The progenitors to such galaxies had a median stellar mass $\log M_*/M_\odot = 10.21$ at $z = 1.1 - 1.4$.[3] These abundance matching methods give stellar mass ≈0.2 dex lower than those selected at constant co-moving number density at these redshifts.[41] More recent work shows that progenitors of Milky Way-mass galaxies span a range of stellar mass at $z = 1.2$, with a 30th to 70th-tile range of $\log M = 10.05$ to 10.34, and a median value consistent with the median above.[42] While observations of CO in $z > 1$ galaxies have probed stellar masses down to $\log M_*/M_\odot > 10.4$,[10] these correspond to the more massive progenitors of present-day Milky Way-mass galaxies. Our sample extends studies of the CO emission to the median stellar mass of progenitors of present-day Milky Way galaxies.

We also selected galaxies with the typical SFRs of the Milky Way-mass progenitors for observations with ALMA. In our previous work we used deep *Spitzer* and *Herschel* imaging to measure an average total IR luminosity, $L_{\rm IR} = (2.0 \pm 0.1) \times 10^{11}$ $L_\odot$, for all Milky Way-mass progenitor galaxies in this redshift and stellar mass range in ZFOURGE.[3] This corresponds to a SFR $= 21 \pm 2$ $M_\odot$ yr^{-1}.

In summary, we used the following criteria to select targets for ALMA:

1. Photometric redshift, $1.1 < z < 1.4$;
2. Stellar mass, $-0.15 < \log M_*/M_\odot - 10.2 < +0.15$;
3. SFR, $-0.15 < \log {\rm SFR}/M_\odot$ yr$^{-1} - 1.3 < +0.15$;
4. measured spectroscopic redshift.

The restrictions on photometric redshift, stellar mass, and SFR select galaxies with stellar mass and SFR within 0.15 dex (i.e., within 40%) of the expected median values of the progenitors to Milky Way-mass galaxies.

The final selection criteria requires that the galaxies have a redshift measured from spectroscopy. This ensures that the redshift accuracy is sufficient for the redshifted CO(3–2) emission line to fall within the frequency range of an ALMA spectral window. While the ZFOURGE photometric redshifts are good ($\sigma_z/(1+z) < 1\%$)[24], these are not sufficient for this purpose.

Of the 24,690 galaxies in the full ZFOURGE catalogue, 39 satisfied the first three selection criteria. At the time of our proposal for ALMA for cycle 2 observations (2013 December), 7 galaxies satisfied all our

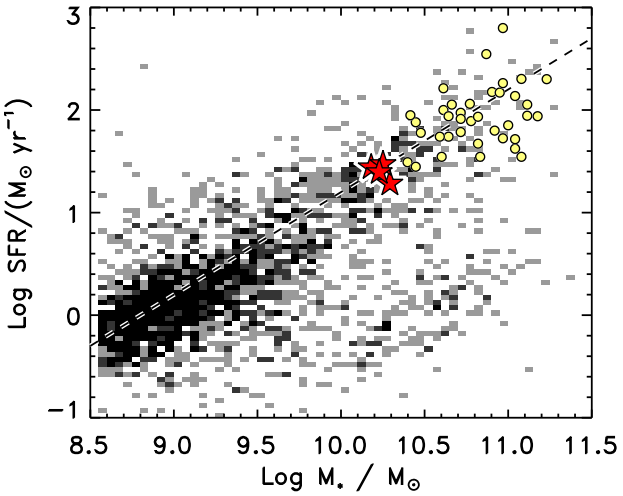

Supplementary Figure 1 | SFR–stellar mass sequence for ZFOURGE galaxies at $1.1 < z < 1.4$**.** The shading increases with the number density of galaxies in each bin. The "main sequence" of star-formation is indicated by the dashed line, and has a slope of SFR $\propto M_*$.[43] The large red stars indicate the four sources selected as typical of main progenitors of Milky Way-mass galaxies at $z = 1.2 - 1.3$ observed with ALMA here. The yellow circles indicate objects with $1.0 < z < 1.5$ with CO detections from PHIBSS.[10]

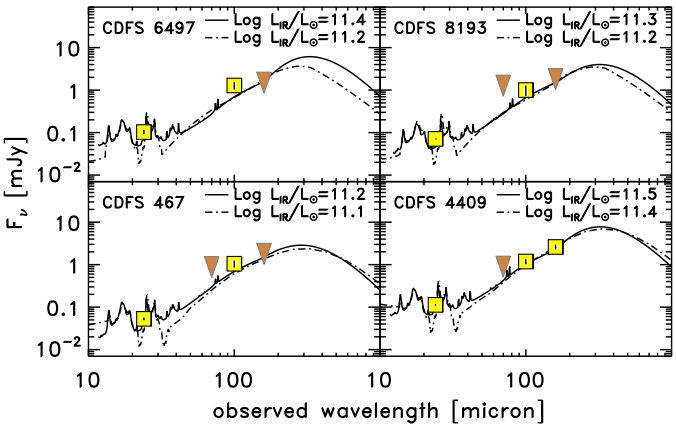

Supplementary Figure 2 | IR Spectral Energy Distribution Model Fits to the far-IR data. The yellow squares show the *Spitzer* 24 μm, and *Herschel* 70, 100, and 160 μm flux densities measured for each object. Error bars are 1σ uncertainties. Downward triangles indicate 3σ upper limits for sources detected with S/N < 3 at that wavelength. The curves show model fits for the Rieke et al.[44] (solid lines) and Chary & Elbaz[45] (dot–dashed lines), which bracket the range of values for total IR luminosity, $L_{\rm IR}$.

Supplementary Table 1: Summary of Far-IR Flux Densities

ZFOURGE ID:	467	4409	6497	8193
$F_\nu(24\mu{\rm m})$:	53 (4)	113 (5)	103 (12)	71 (12)
$F_\nu(70\mu{\rm m})$:	<1.2	<0.9	...	<1.4
$F_\nu(100\mu{\rm m})$:	1.1 (0.2)	1.2 (0.2)	1.3 (0.3)	1.0 (0.3)
$F_\nu(160\mu{\rm m})$:	<2.0	2.6 (0.3)	<1.7	<2.1

Numbers in parentheses are 1σ uncertainties. 24 μm flux densities are in units of μJy. All other flux densities are in units of mJy, where 1 μJy = 10^{-3} mJy, and 1 mJy = 10^{-26} erg s^{-1} cm^{-2} Hz^{-1}. Upper limits are 3σ.

Supplementary Table 2: Summary of ALMA observations

ZFOURGE ID[a]	Obs. Dates	PMV[b] (mm)	$T_{\rm int}$[c] (min)	Frequency Range (GHz)	Combined Beam[d]	FWHM[e] (km s^{-1})	$\sigma^{\rm f}_{\rm r.m.s.}$ (mJy beam^{-1})
CDFS 467 (8769)	2015 Apr 7	3.2	37.3	140.9–156.6	$3\farcs5 \times 1\farcs3$, P.A. = -74.1°	240 (120)	0.42
CDFS 4409 (19996)	2015 Apr 7	3.6	37.3	140.9–156.6	$2\farcs4 \times 1\farcs4$, P.A. = -85.8°	440 (150)	0.42
CDFS 6497 (24956)	2015 May 2	1.0	37.8	141.3–156.9	$2\farcs7 \times 1\farcs3$, P.A. = -77.9°[,g]	310 (50)[g]	0.33[g]
	2015 May 2	1.5	37.8	141.3–156.9			
CDFS 8193 (28279)	2015 Apr 6	4.6	41.8	134.5–149.5	$2\farcs8 \times 1\farcs4$, P.A. = -81.7°	54 (16)	0.48

[a]Source ID in the previous ZFOURGE v2.1 proprietary catalogues used to select targets for ALMA. The numbers in parentheses are the ZFOURGE source ID in the public v3.4 catalogues.[24] [b]Estimated precipitable water vapour. [c]On-source integration time. [d]FWHM and orientation of cleaned beam (numbers in parentheses are 1σ uncertainties). These are displayed graphically in figure 1. [e]The FWHM of the CO(3-2) line in the measured spectrum. [f]R.M.S. noise per channel measured in primary-beam corrected data. [g]For this object, the beam size, FWHM, and noise are measured from the combined, 2-epoch dataset.

selection criteria (including having a published spectroscopic redshift in the literature).[25] From these, we selected four objects offering some contrast in SFR (spanning nearly 0.3 dex). For the analysis in this Letter, we rederived stellar masses and uncertainties using FAST [46] with an extended stellar population library (including a broader metallicity range of $0.2 - 1.0\ Z_\odot$ and a finer grid spacing of star-formation histories) compared to the one used for the ZFOURGE catalogues.[24] These stellar masses and 68% likelihood range are listed in Table 1, and are consistent with those in the v2.1 and v3.4 ZFOURGE catalogues.

All four galaxies selected for ALMA observations have properties characteristic of the typical properties of progenitors to a Milky Way-mass galaxy at $z = 1.2-1.3$. Supplementary Figure 1 shows the SFR–stellar mass relation for galaxies from ZFOURGE with $1.1 < z < 1.4$. Galaxies with the stellar mass and and SFR of the Milky Way-mass progenitors lie on the star-forming "main sequence",[43] and this includes the four galaxies we observed with ALMA. Therefore, they correspond to a typical star-forming galaxy at these redshifts. Previous studies of CO emission in galaxies at these redshifts have been limited to higher SFRs ($\gtrsim$30 $M_\odot$ yr^{-1}) and/or stellar masses (M_*>2.5×10^{10} $M_\odot$)[9,10]. As illustrated in Supplementary Figure 1, the observations of our sample with ALMA provide an important extension compared to previous studies. Furthermore, previous studies required up to 25 hrs of integration with IRAM PdBI to detect galaxies at these mass and SFR limits.[10] Our ALMA observations required only $\simeq$40 min, demonstrating the efficacy of ALMA for this science.

3 Far–IR data and IR Luminosities

The ZFOURGE fields include imaging at far–IR wavelengths from *Spitzer*/MIPS (24 μm), *Herschel*/PACS (70, 100, and 160 μm). Fluxes are measured in these data using source detections based on prior locations of sources in *HST*/WFC3 F160W (1.6 μm) data using methods identical to those described elsewhere.[47–49] We measured flux uncertainties and evaluated source completeness through extensive artificial object simulations, following the same procedures discussed elsewhere[49,50] The 24–160 μm flux densities for the four objects studied here are listed in Table S1. (Note that one source, ZFOURGE CDFS 4409, has no coverage by PACS 70 μm).

In all cases, the IR flux densities and flux uncertainties that we measure for our sources are consistent with other published values,[47,51] available on the WWW (http://irsa.ipac.caltech.edu/data/Herschel/PEP). In many cases, our measured flux densities at 70 μm and 160 μm have S/N<3. While formally undetected, we include this information in our analysis as it provides important constraints on the total IR emission from these galaxies.

To measure total IR luminosities, $L_{\rm IR}$, we fit models of the IR spectral energy distribution[44,45,52] to the flux densities in Table S1. Because the data sample well the Wein side of the thermal emission, the constraints on the IR luminosity are quite robust. Supplementary figure 2 shows the fits using the Chary & Elbaz and Rieke et al. models,[44,45] which bracket the range of values. The slight differences in IR spectral energy distribution shape lead to systematically different IR luminosities, where $L_{\rm IR}$ from the Rieke et al. templates are higher by $\Delta(\log L_{\rm IR})$ = 0.1–0.2 dex. We have also calculated IR luminosities ignoring data where objects are detected at $<2\sigma$, but this produces changes in the IR luminosities by <15% in most cases. We therefore adopt the $L_{\rm IR}$ from the fits to the Rieke et al. models to all the IR data, which we report in Table 1. If we instead adopt the results from the fits to the Chary & Elbaz models, the star-formation efficiencies (SFEs) would decline, and gas consumption timescales would increase for the $z = 1.2 - 1.3$ galaxies in our sample studied here. This would bring the SFEs further in line with local spiral galaxies, strengthening that conclusion.

The total IR luminosities for the z=1.2–1.3 galaxies in our sample span $L_{\rm IR}$=$(1.5 - 3.2)\times10^{11}$ $L_\odot$, as listed in Table 1. In these galaxies, most of the bolometric emission from star formation is emitted in the thermal IR. In constrast, we measure that the rest-frame UV (uncorrected for dust extinction) contributes only 4–6% to the total SFR implied by the $L_{\rm IR}$ in these galaxies. This is consistent with mean values measured in local luminous IR galaxies.[53]

4 ALMA Observations and Data Reduction

Our Cycle 2 ALMA observations were taken between 2015 April 6 and 2015 May 2 in Band 4 with 36 antennas in the C34-2 configuration, which provided a maximum baseline of 348.5 m. For each source, we configured ALMA to observe in four spectral windows, 1.875 GHz per window, and spanning frequencies 134.48 to 156.90 GHz (depending on the expected frequency of the CO[3–2] transition for each source). We centered the CO(3–2) line in one of the spectral windows assuming the optical spectroscopic redshift from the literature.[25] The ALMA integrations ranged between 37.3 to 41.8 min on source. One source (ZFOURGE CDFS 6497) was erroneously observed twice, and received double the exposure time. The other spectral windows probe the continuum of the line. Flux, phase, and band-pass calibrators were also obtained. Supplementary Table 2 provides details about the observations for each source.

We reduced the data with CASA (Common Astronomy Software Applications[54]) version 4.5.0-REL with the calibration script supplied by the National Radio Astronomy Observatory (NRAO). We then ran the cleaning algorithm with natural weighting. For the spectral window containing the CO(3–2) line, we reduced the data with channels of 25 km s^{-1} and 75 km s^{-1} with a cell size of $0\farcs2$. The angular sizes of the cleaned beam FWHM are given in Table S2, and this cell size gives 6–7 cells along the semi-minor axis of the beam.

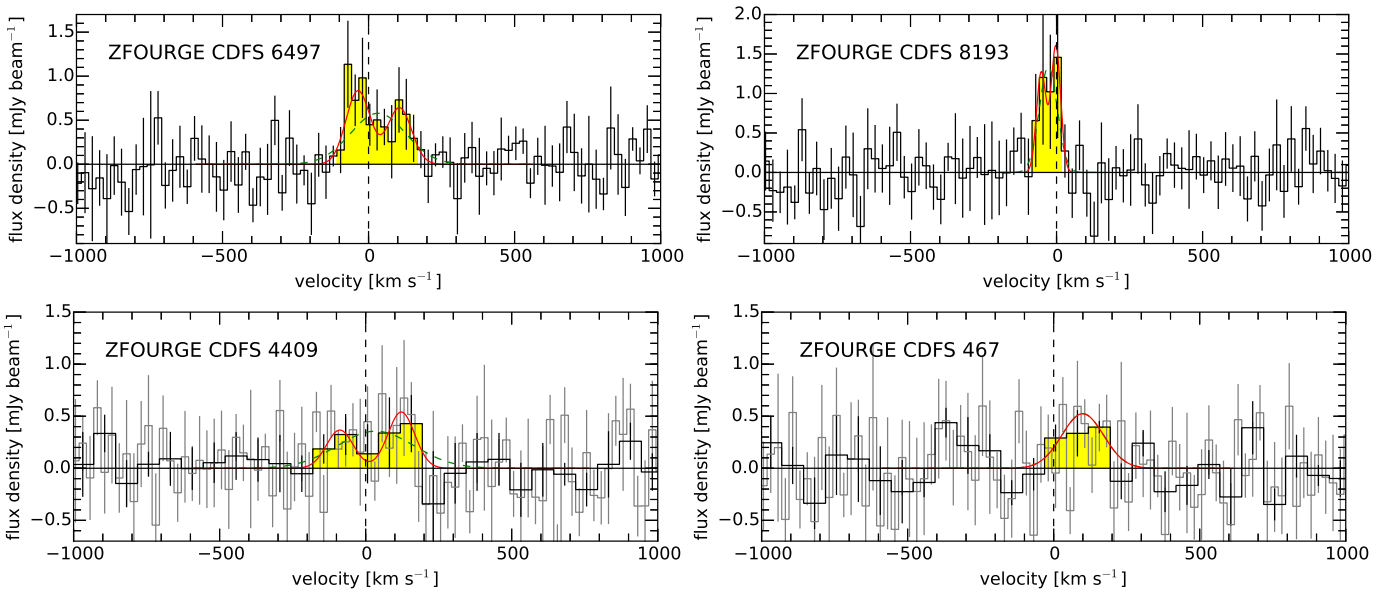

Supplementary Figure 3 | Spectra of CO(3–2) for the $\log M_*/M_\odot \simeq$ 10.2 galaxies at redshifts z = 1.2 to 1.3. In each panel, the spectra are shown in 25 km s^{-1} channels. For objects ZFOURGE 467 and 4409, the heavier-lined spectra are in 75 km s^{-1} channels to improve S/N. The yellow-shaded regions indicate channels where postive emission is detected at the expected location of the line. In each panel, the velocity is measured relative to the expected location of the line from the optical spectroscopic redshift. There are two fits to each CO(3–2) line. The green line shows a model with a single Gaussian. The red line shows a model with two Gaussians.

We also attempted to measure the continuum for each galaxy by cleaning and combining the spectral windows excluding channels expected to have CO emission. We failed to detect any signal of the continuum; we also therefore made no correction for the continuum to the CO line fluxes.

Supplementary figure 3 shows the spectra of the CO(J=3–2) emission for the four galaxies. For each galaxy, there is positive emission in the channels at the expected location of the CO(3–2) line. To determine the peak of emission we fit the spectra with models using single- and double-Gaussians. The velocity offsets between the CO redshift and redshift from the optical spectroscopy range from -30 to $+100$ km s^{-1}. This is consistent with uncertainties in the redshift measurements.

We created total intensity maps of the CO(3–2) lines in each galaxy by combining the channels showing positive emission around the expected position of each line. We also created first moment (velocity) and second moment (velocity dispersion) maps to study galaxy gas dynamics. From the primary-beam-corrected, total intensity maps, we measured integrated flux densities for the CO(3–2) transition, $I_{\rm CO(3-2)}$, for each galaxy in our sample using the two-dimensional profile fitting tool in CASA. These are presented in Table 1, and range from $I_{\rm CO(3-2)}$=0.11–0.33 Jy km s^{-1}. While the S/N of the integrated values in Table 1 range from 2.3–7.7, the detection significance (measured from the peak of the emission) is much higher, where the S/N ranges from 4.8 to 13.7.

As discussed in the next section, the ALMA spectra in Supplementary figure 3 show evidence for complex velocities, except for ZFOURGE CDFS 467, where the data quality is lower. The spectrum of this object does show tentative, weak emission to the blue side of the systemic redshift (at velocities -400 to -200 km s^{-1}). However, the integrated emission from these channels is not significant, having a S/N of $\simeq$2.0 at the peak. When the emission from the blue-side channels is summed with that on the red side (where the object is detected), it lowers the overall significance of the detection from 4.8 to 3.0. We therefore do not include this emission in the analysis of this object. However, including it would increase the CO luminosity by a factor of 1.6, making it more consistent with the other objects in the sample.

5 Velocity Shear in CO Emission

Our analysis of the spectra of the CO(3–2) emission in the four $z = 1.2 - 1.3$ galaxies in our sample in Supplementary figure 3 shows that in many cases a double–Gaussian model fits better reproduce the data than the single–Gaussian models. This is consistent with the expected signature of rotation. Further evidence comes from observations of velocity shear in the galaxies: some galaxies show spatial variations in their velocity components. For three of the galaxies with the strongest emission, (ZFOURGE CDFS 4409, 6497, 8193) we measured total CO(3–2) intensity maps separately from the channels blueward (approaching) and redward (receding) relative to the velocity with the minimum emission between the peaks. Two of these galaxies (ZFOURGE 6497 and 8193) show velocity shear (in the third object the signal–to–noise is too low to centroid robustly the two separate components). Supplementary figure 4 shows there are spatial offsets in the centroids of the emission in the red and blue components in these galaxies. While the beam size precludes accurate modelling of the velocity shear, the spatial variations are consistent with rotation.

Taken together, the CO spectra and spatial separation of the approaching and receding velocity components provide reasonable evidence for rotation in the $z = 1.2 - 1.3$ galaxies in our sample. While the presence of double-peaked velocity structures in the CO spectra could be expected for merging systems, we consider this unlikely for two reasons. First, the *HST* morphologies of the galaxies in our sample (see Figure 1) show no indications of double nuclei, which would be expected if a merger was responsible for the CO velocity structure. Second, the galaxies in our sample lie on the "main-sequence" of the SFR–M_* relation (Supplementary figure 1), and they show no indications of merger–induced starbursts on their star-formation efficiencies, $L_{\rm IR}/L'({\rm CO})$ (Figure 2). Direct confirmation of rotation in these galaxies would require higher spatial resolution kinematic data which is possible from ALMA in larger configurations, but requires considerably more exposure time.

6 Molecular Gas mass from CO emission

The observed CO luminosity is proportional to the total cold molecular gas mass, $M_{\rm gas}$. At the temperatures and pressures of the ISM in

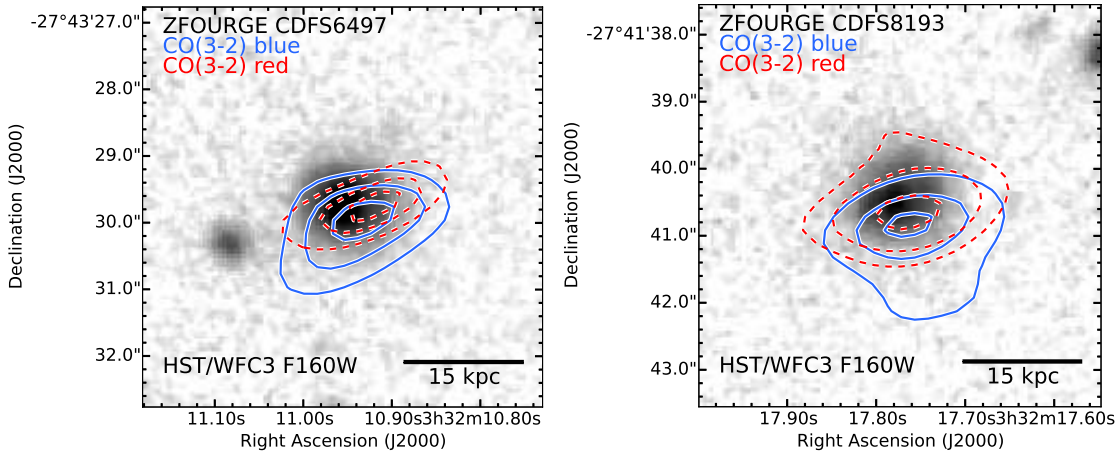

Supplementary Figure 4 | CO(3–2) maps of two galaxies with velocity shear: spatial offsets in their velocity components. The contours show the CO(3–2) emission from the blue-shifted (approaching) and red-shifted (receding) emission. The contours are overdrawn on the HST/WFC3 F160W images from CANDELS.[36,37]

our galaxies, we expect that most of the gas exists in the molecular phase,[55] and therefore the molecular gas accounts for the majority of baryons in the gas phase. The constant of proportionality (the gas-mass–to–light ratio), $\alpha_{\rm CO}$, is given by

$$\alpha_{\rm CO} = M_{\rm gas}/L'({\rm CO}). \quad (1)$$

Based on the $L_{\rm IR}/L'({\rm CO})$ ratios, the conditions in the z=1.2–1.3 galaxies in our sample appear similar to normal star-forming regions and star-forming disk galaxies, which show values of $\alpha_{\rm CO} \sim 4\ M_\odot$ (K km s^{-1} pc^2)$^{-1}$,[32] and traces the total amount of molecular gas including a correction for helium.[56] The CO–to–molecular gas conversion factor is α=4.3 $M_\odot$ (K km s^{-1} pc^2)$^{-1}$ for star-forming regions in the Galaxy and in "normal" star-forming galaxies.[56] The galaxies in our sample have $L_{\rm IR}/L'({\rm CO})$ ratios consistent with other normal star-forming galaxies (see figure 2). We therefore adopt $\alpha_{\rm CO} = 3.6\ M_\odot$ (K km s^{-1} pc^2)$^{-1}$ found to apply to normal star-forming (more massive) galaxies at these redshifts, and contains a calibration uncertainty of 22%.[7]

There is evidence that the CO–to–molecular gas ratio, $\alpha_{\rm CO}$, varies with metallicity, Z, where the values in the discussion above correspond to Solar values, Z=$Z_\odot$. Theoretical work predicts that $\alpha_{\rm CO} \propto Z^{-0.5}$,[57,58] while empirical measurements at redshifts $z > 1$ suggest a possible steeper relation, $\alpha_{\rm CO} \propto Z^{-1.2}$ to $Z^{-1.8}$.[59] If the galaxies in our ALMA sample have Z<$Z_\odot$, one may expect an increase in $\alpha_{\rm CO}$. Work on the stellar-mass—metallicity (M^*–Z) relation at $0.9 < z < 1.3$ shows that star-forming galaxies in the mass range of our sample should have metallicities between 0.6–1.0 $Z_\odot$.[60–62] This implies a higher $\alpha_{\rm CO}$ (and higher gas masses) by at most a factor of $\sim$2. This would correspond to even more dramatic evolution in the gas fraction from $z \sim 1.3$ to the present for Milky-way mass galaxies. For this reason, we adopt the (more conservative) CO–to-molecular gas ratio for Solar metallicity, $\alpha_{\rm CO} = 3.6\ M_\odot$(K km s^{-1} pc^2)$^{-1}$, as stated in the discussion above.

7 Conventions

Throughout, we assume a Chabrier initial mass function[63] when deriving stellar masses and SFRs. For all cosmological calculations, we assume $\Omega_m = 0.3$, $\Omega_\Lambda = 0.7$, and $H_0 = 70$ km s^{-1} Mpc^{-1}, consistent with the recent constraints from Planck[64] and the local distance scale.[65]

35. Persson, S. E. *et al.* FourStar: The Near-Infrared Imager for the 6.5 μ m Baade Telescope at Las Campanas Observatory. *Publ. Astron. Soc. Pac.* **125**, 654–682 (2013).
36. Grogin, N. A. *et al.* CANDELS: The Cosmic Assembly Near-infrared Deep Extragalactic Legacy Survey. *Astrophys. J. Supp.* **197**, 35 (2011).
37. Koekemoer, A. M. *et al.* CANDELS: The Cosmic Assembly Near-infrared Deep Extragalactic Legacy Survey — The Hubble Space Telescope Observations, Imaging Data Products, and Mosaics. *Astrophys. J. Supp.* **197**, 36 (2011).
38. Tomczak, A. R. *et al.* Galaxy Stellar Mass Functions from ZFOURGE/CANDELS: An Excess of Low-mass Galaxies since z = 2 and the Rapid Buildup of Quiescent Galaxies. *Astrophys. J.* **783**, 85 (2014).
39. Mutch, S. J., Croton, D. J. & Poole, G. B. The Mid-life Crisis of the Milky Way and M31. *Astrophys. J.* **736**, 84 (2011).
40. Moster, B. P., Naab, T. & White, S. D. M. Galactic star formation and accretion histories from matching galaxies to dark matter haloes. *Mon. Not. R. Astron. Soc.* **428**, 3121–3138 (2013).
41. van Dokkum, P. G. *et al.* The Assembly of Milky-Way-like Galaxies Since z ˜ 2.5. *Astrophys. J. Let.* **771**, L35 (2013).
42. Wellons, S. & Torrey, P. An improved probabilistic approach for linking progenitor and descendant galaxy populations using comoving number density. *MNRAS, submitted (preprint arXiv:1606.07815)* (2016).
43. Tomczak, A. R. *et al.* The SFR-M* Relation and Empirical Star-Formation Histories from ZFOURGE* at 0.5 < z < 4. *Astrophys. J.* **817**, 118 (2016).
44. Rieke, G. H. *et al.* Determining Star Formation Rates for Infrared Galaxies. *Astrophys. J.* **692**, 556–573 (2009).
45. Chary, R. & Elbaz, D. Interpreting the Cosmic Infrared Background: Constraints on the Evolution of the Dust-enshrouded Star Formation Rate. *Astrophys. J.* **556**, 562–581 (2001).
46. Kriek, M. *et al.* An Ultra-Deep Near-Infrared Spectrum of a Compact Quiescent Galaxy at z = 2.2. *Astrophys. J.* **700**, 221–231 (2009).
47. Elbaz, D. *et al.* GOODS-Herschel: an infrared main sequence for star-forming galaxies. *Astron. Astrophys.* **533**, A119 (2011).
48. Magnelli, B. *et al.* Evolution of the dusty infrared luminosity function from z = 0 to z = 2.3 using observations from Spitzer. *Astron. Astrophys.* **528**, A35 (2011).
49. Magnelli, B. *et al.* The deepest Herschel-PACS far-infrared survey: number counts and infrared luminosity functions from combined PEP/GOODS-H observations. *Astron. Astrophys.* **553**, A132 (2013).
50. Berta, S. *et al.* PEP full public data release (DR1): PACS data. *http://irsa.ipac.caltech.edu/data/Herschel/PEP/docs/readme%5FPEP%5Fglobal.pdf* (2013).
51. Lutz, D. *et al.* PACS Evolutionary Probe (PEP) - A Herschel key program. *Astron. Astrophys.* **532**, A90 (2011).
52. Dale, D. A. *et al.* Infrared Spectral Energy Distributions of Nearby Galaxies. *Astrophys. J.* **633**, 857–870 (2005).
53. Howell, J. H. *et al.* The Great Observatories All-sky LIRG Survey: Comparison of Ultraviolet and Far-infrared Properties. *Astrophys. J.* **715**, 572–588 (2010).
54. McMullin, J. P., Waters, B., Schiebel, D., Young, W. & Golap, K. CASA Architecture and Applications. In Shaw, R. A., Hill, F. & Bell, D. J. (eds.) *Astronomical Data Analysis Software and Systems XVI*, vol. 376 of *Astronomical Society of the Pacific Conference Series*, 127 (2007).
55. Daddi, E. *et al.* Different Star Formation Laws for Disks Versus Starbursts at Low and High Redshifts. *Astrophys. J. Let.* **714**, L118–L122 (2010).
56. Bolatto, A. D., Wolfire, M. & Leroy, A. K. The CO-to-H_2 Conversion Factor. *Annu. Rev. Astron. Astrophys.* **51**, 207–268 (2013).

57. Feldmann, R., Gnedin, N. Y. & Kravtsov, A. V. The X-factor in Galaxies. I. Dependence on Environment and Scale. *Astrophys. J.* **747**, 124 (2012).
58. Narayanan, D., Krumholz, M. R., Ostriker, E. C. & Hernquist, L. A general model for the CO-H_2 conversion factor in galaxies with applications to the star formation law. *Mon. Not. R. Astron. Soc.* **421**, 3127–3146 (2012).
59. Genzel, R. *et al.* The Metallicity Dependence of the $CO - H_2$ Conversion Factor in $z > 1$ Star-forming Galaxies. *Astrophys. J.* **746**, 69 (2012).
60. Pérez-Montero, E. *et al.* Physical properties of galaxies and their evolution in the VIMOS VLT Deep Survey. II. Extending the mass-metallicity relation to the range $z \sim 0.89$-1.24. *Astron. Astrophys.* **495**, 73–81 (2009).
61. Zahid, H. J., Kewley, L. J. & Bresolin, F. The Mass-Metallicity and Luminosity-Metallicity Relations from DEEP2 at z ˜ 0.8. *Astrophys. J.* **730**, 137 (2011).
62. Stott, J. P. *et al.* A fundamental metallicity relation for galaxies at z = 0.84-1.47 from HiZELS. *Mon. Not. R. Astron. Soc.* **436**, 1130–1141 (2013).
63. Chabrier, G. Galactic Stellar and Substellar Initial Mass Function. *Publ. Astron. Soc. Pac.* **115**, 763–795 (2003).
64. Planck Collaboration *et al.* Planck 2015 results. XIII. Cosmological parameters. *preprint, arXiv:1502.01589* (2015).
65. Riess, A. G. *et al.* A 2.4% Determination of the Local Value of the Hubble Constant. *Astrophys. J., submitted, arXiv:1604.01424* (2016).